LETTERS
PUBLISHED ONLINE: 23 DECEMBER 2012 | DOI: 10.1038/NNANO.2012.218
nature nanotechnology

Controlled clockwise and anticlockwise rotational switching of a molecular motor

U. G. E. Perera[1], F. Ample[4], H. Kersell[1], Y. Zhang[1], G. Vives[2], J. Echeverria[2], M. Grisolia[2], G. Rapenne[2,3]*, C. Joachim[2,4]* and S-W. Hla[1]*

The design of artificial molecular machines[1–19] often takes inspiration from macroscopic machines[13–19]. However, the parallels between the two systems are often only superficial, because most molecular machines are governed by quantum processes. Previously, rotary molecular motors[3] powered by light[4–6] and chemical[7–11] energy have been developed. In electrically driven motors, tunnelling electrons from the tip of a scanning tunnelling microscope have been used to drive the rotation of a simple rotor[12] in a single direction and to move a four-wheeled molecule across a surface[13]. Here, we show that a stand-alone molecular motor adsorbed on a gold surface can be made to rotate in a clockwise or anticlockwise direction by selective inelastic electron tunnelling through different subunits of the motor. Our motor is composed of a tripodal stator for vertical positioning, a five-arm rotor for controlled rotations, and a ruthenium atomic ball bearing connecting the static and rotational parts. The directional rotation arises from sawtooth-like rotational potentials, which are solely determined by the internal molecular structure and are independent of the surface adsorption site.

Our molecular motor comprises a piano-stool complex [η^5-1-(4-tolyl)-2,3,4,5-tetra(4-ferrocenylphenyl) cyclopentadienyl hydrotris [6-((ethylsulphanyl)methyl)indazol-1-yl] borate ruthenium(II)][18] consisting of a five-arm rotor mounted on a molecular tripodal stator (Fig. 1a,b). Rotation of the rotor is enabled by the central ruthenium atom acting as an atomic ball bearing between the stator and the central five-membered ring in the rotor[19]. Four of the rotor arms have a ferrocene group attached at their ends, and the fifth arm is truncated beyond the phenyl ring. This provides a structural dissymmetry that helps in the detection of discrete rotation steps of the rotor relative to the stator. Ferrocene groups were chosen for their electro-activity, which enables them to act as reversible electron relays. To provide vertical stability, each leg of the stator is tethered to the surface by a thioether group (SEt, a sulphur atom bearing an ethyl substituent). The ferrocene end groups were added to facilitate planar control of the rotation of the motor using a system of four metallic nanoelectrodes[20].

The scanning tunnelling microscope (STM) is a useful tool for probing the rotation of molecules on surfaces at the single-molecule level[21–29]. Our STM experiments were performed using a custom-built ultrahigh-vacuum, low-temperature STM system operating at a base pressure below 4×10^{-11} torr (ref. 26). An electrochemically etched polycrystalline tungsten wire was used as the STM tip.

A single-crystal Au(111) sample was cleaned by repeated cycles of neon ion sputtering and annealing to 700 K. The molecular motors were deposited on a cleaned Au(111) sample (held at ~120 K) by thermal evaporation (source temperature, 450 K) using a custom-built Knudsen cell in an ultrahigh-vacuum environment. The sample was then transferred to the STM chamber *in situ*. Subsequently, the sample temperature was lowered to 80 K or 4.6 K for different experiments.

STM images acquired at a substrate temperature of 80 K show scattered individual molecular motors mostly located at the edges of the herringbone surface reconstructions, and the rotor of the motor appears to be freely rotating at this temperature (Fig. 1c,d). Lowering the surface temperature further brings the rotation to a halt, and images taken at 4.6 K show the five-lobe structure of the dissymmetric rotor, which comprises four ferrocene groups and the truncated arm (Fig. 1e).

It was imperative to first determine whether a complete motor setup was in place on the surface. This could be achieved by removing the top rotor part so that the existence of the base stator unit could be confirmed. This was realized by removing the rotor using a large bias voltage pulse (−2.3 V) applied to the STM junction (Fig. 1f) (Supplementary Section S5). The tripodal stator could then be observed standing on the surface. Although this process could not determine whether all the atoms were in place, the existence of the tripod underneath the rotor as well as the vertically upright positioning of the motor on the surface could be confirmed. Moreover, examination of the tripod also allowed us to establish the location of the molecular adsorption site, with each stator leg positioned along a [211] surface direction of the Au(111) (Fig. 1f).

STM manipulation and spectroscopy were then used to explore rotational switching of the molecular motor. The excitation energy threshold required for rotation was first determined by positioning the STM tip above the centre of the rotor, then gradually increasing the tunnelling voltage. The recorded I–V spectrum shows a sudden increase in tunnelling current at ~0.6 V, followed by a fluctuation of current associated with rotation (Fig. 2a). STM images confirmed rotational switching of the top rotor part (Fig. 3). As this 0.6 V energy range is approaching the lowest excited states of the molecular motor (Fig. 2b), this rotation can be explained as being triggered by an inelastic electron energy transfer when tunnelling through the excited states[21,27–29].

Although the molecule begins to rotate above 0.6 V, rotations in both clockwise and anticlockwise directions can be realized by exciting any arm of the rotor only when the tunnelling electron energy exceeds 1.8 eV. Accordingly, stepwise rotations were performed at 4.6 K on a stationary molecular motor by positioning the STM tip above the molecule at a fixed height, then initiating tunnelling through the electronic excited states with energy up to 1.8 eV for a few seconds. During this process, an abrupt change in tunnelling current (Fig. 2c) is associated with a rotation step. This rotation is

[1]Nanoscale and Quantum Phenomena Institute, Physics & Astronomy Department, Ohio University, Athens, Ohio 45701, USA, [2]GNS & MANA Satellite, CEMES, CNRS, 29 rue J. Marvig, 31055 Toulouse Cedex, France, [3]Université de Toulouse, UPS, 118 route de Narbonne, 31062 Toulouse, France, [4]IMRE, A*STAR (Agency for Science, Technology and Research), 3 Research Link, 117602, Singapore. *e-mail: hla@ohio.edu; joachim@cemes.fr; rapenne@cemes.fr

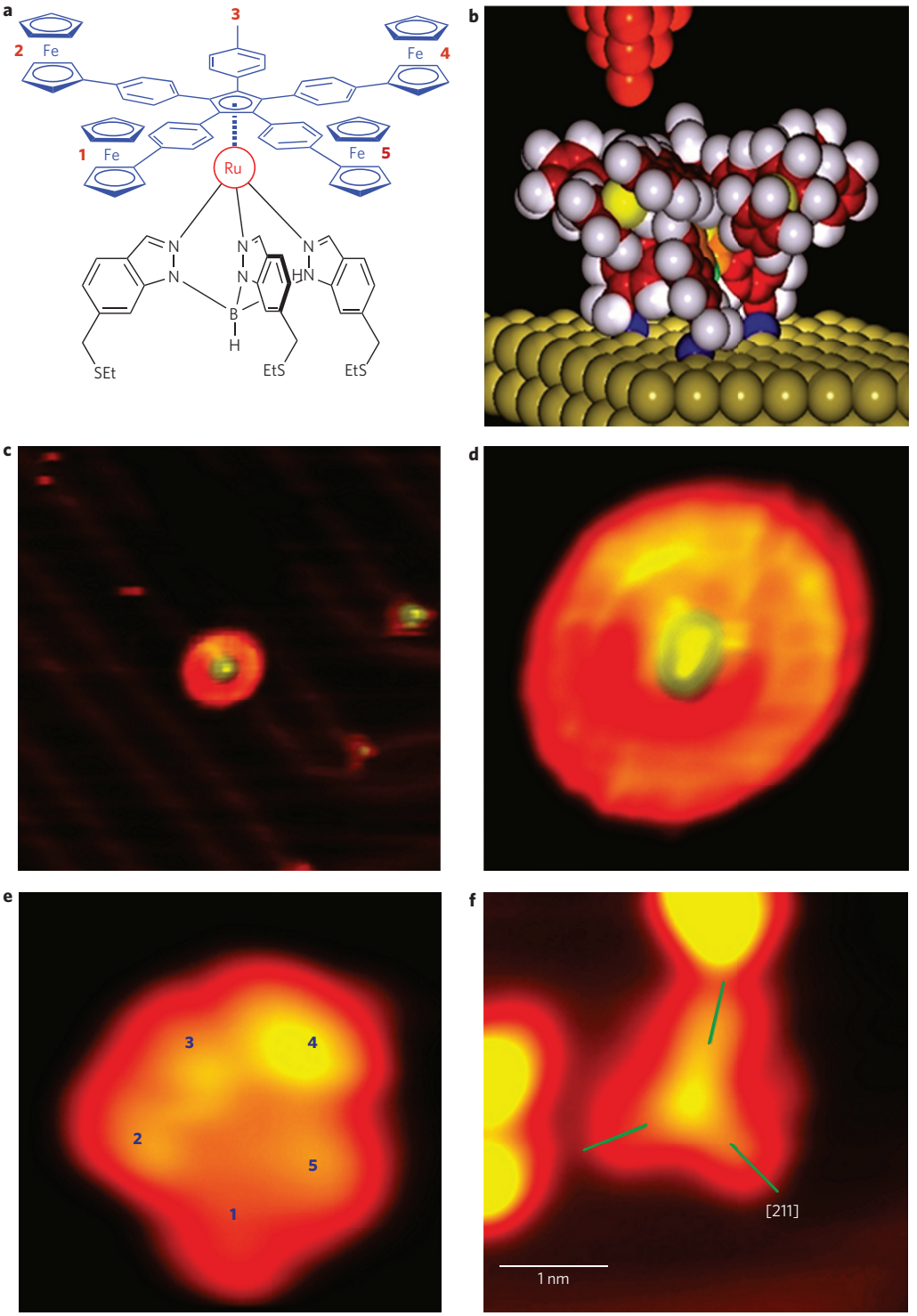

Figure 1 | Structure of the molecular motor. a, Chemical structure of the motor. **b**, Three-dimensional representation of an optimized motor structure on Au(111). **c**, A rotating motor on Au(111) together with background herringbone reconstruction (diagonal lines) ($V_t = -1.2$ V, $I_t = 0.28$ nA, 15 nm × 15 nm). **d**, Close-up view of a rotating motor at 80 K ($V_t = -1.3$ V, $I_t = 0.28$ nA, 3.6 nm × 3.6 nm). **e**, Close-up view of a stationary motor at 4.6 K ($V_t = -1$ V, $I_t = 0.23$ A, 3.3 nm × 3.3 nm). Labels 1, 2, 4 and 5 are the ferrocene-terminated arms and 3 is the truncated arm, as shown in **a**. **f**, A tripodal structure of the stator is observed after removing the top rotor part of the motor, which shows orientation of the legs along [211] surface directions.

based on electronic excitation by means of tunnelling electron energy transfer to the molecule. The number of stepwise rotational switching events decays exponentially with time, and the rotation rate can be deduced from a plot of these events versus time (Fig. 2d). Finally, the data collected over 500 rotational events at four different currents can be used to determine the R versus I^N relationship, where R is the rate, I is the current and N is the number of electrons involved in the process of energy transfer to the molecule (Fig. 2e)[21,27,28]. The slope of a plot of ln R versus ln I gives N, which was determined to be 0.98 ± 0.03. This value is close to unity, indicating that a single tunnelling electron energy transfer induces each step[27–29]. This further indicates that we are

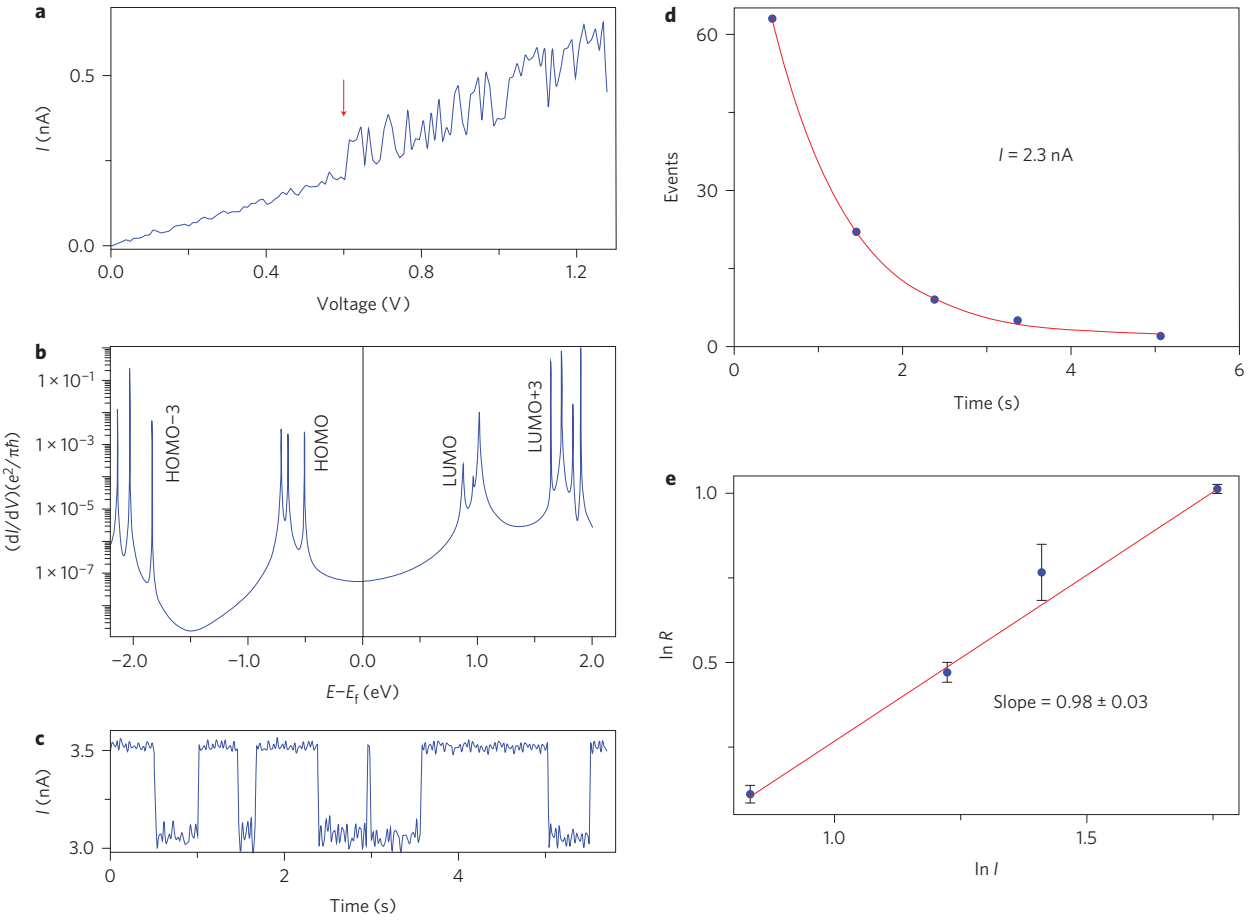

Figure 2 | Rotational energy and electronic structure. a, $I-V$ curve showing a sudden increase in current (indicated by red arrow) due to rotation of the motor. **b**, Calculated dI/dV spectrum with the tip positioned on a ferrocene reveals the molecular orbital contributions to the tunnelling current. **c**, Abrupt changes in tunnelling current are due to rotations. **d**, Number of stepwise rotation events as a function of time, showing an exponential decay. The rotation rate is determined from the exponential fit (red line). **e**, Plot of ln R versus ln I, showing a slope close to unity. Error bars in **e** are standard deviations from the switching rates.

observing an inelastic electron tunnelling (IET) process[27–29]. Single-step rotations are mostly found for short excitation periods of less than 1 s, while multistep rotations are more common for excitation periods of more than 2 s for a tunnelling current range of 0.6 nA (see Supplementary Information).

Figure 3 presents a sequence of experimental and corresponding calculated STM images for rotation achieved using the IET process. The angles of rotation here are multiples of 24°, and the rotation proceeds in single steps. For single-step switching from one conformation to another, rotation can occur in either the clockwise or anticlockwise direction, but preferential rotation has been achieved in both directions depending on the choice of STM tip location above a specific rotor arm. The mean rotation is predominantly clockwise if electrons are passing through truncated arm position 3, and mostly anticlockwise if electron excitation is via a ferrocene arm (Fig. 3). Excitation of a specific subunit of the motor therefore enables a controlled unidirectional rotation if the excitation period is sufficiently long. We have not been able to switch the molecule using negative biases, indicating that the rotation is based on the inelastic excitation of specific excited states of the molecule. As exemplified in Fig. 1f, a negative bias voltage often leads to destruction of the rotor. Moreover, different tips produce similar rotations, so the rotation mechanism here differs from the molecular rotation induced with chiral tips by Tiernary and colleagues[12]. Our controlled rotation process can be performed repeatedly, as shown in Fig. 3.

To explain the observed directional rotation of the motor, calculations were performed using semi-empirical ASED+[30] and density functional theory (DFT) methods. For a 360° rotation of the rotor, there should be 15 potential wells for a five-arm rotor located on top of a three-leg (tripodal) stator. Calculated results for the molecular motor with five ferrocene arms on a two-layer Au(111) slab give a periodic ground-state potential energy with energy minima located at 24° separations (Fig. 4a). The locations of the potential energy maxima are slightly off-centre and thus produce a sawtooth-like rotational potential shape. When the truncated arm is introduced, an asymmetric ground-state potential curve is produced (Fig. 4a) because of the lower symmetry. The sawtooth-like potential is still preserved, which is a necessary condition for a unidirectional rotation[31]. The locations of the molecular orbital density maxima differ not only in their energies, but also in their positions (see Supplementary Information). Because of the large size of the molecule, it is possible to realize selective excitation of a specific subunit of the rotor by positioning the STM tip above the desired orbital location. For instance, the LUMO and LUMO+1 are directly linked to the ruthenium atom joint and are located close to the truncated arm (Fig. 4b). Thus, excitation at this arm position enables the molecule to rotate along the clockwise direction by electron energy transfer via the LUMO and LUMO+1 component of the low-lying excited states. On the other hand, the LUMO+3 to LUMO+6 (Fig. 4c) open tunnelling channels through the ferrocene arm.

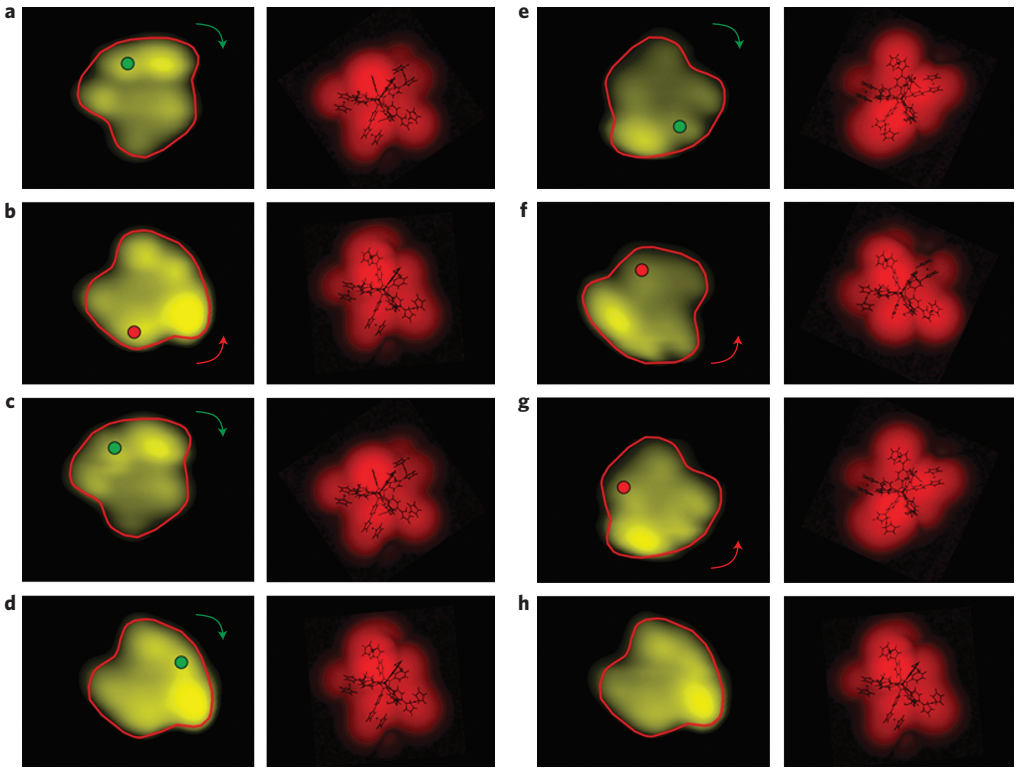

Figure 3 | Controlled rotation. a–h, Sequence of STM images revealing multistep rotations of the rotor induced by tunnelling electrons. The green dot is the tip position above the truncated arm, which results in clockwise rotations in the next image (−1 V, 0.34 nA, 4.6 nm × 3.7 nm). The red dot is the tip position on a ferrocene arm, leading to anticlockwise rotations in the next image. Calculated STM images are in red. Angles between panels: **ab**, **bc**, **cd** = 72°; **de**, **gh** = 96°; **ef**, **fg** = 48°.

Interestingly, the potential energy curves of the LUMO+5 and LUMO+6 also appear as sawtooth shapes, but in a reverse direction relative to the ground-state potential (Fig. 4a), which allows rotation in the opposite direction when excited through a ferrocene arm (Fig. 3). When the electrons are tunnelling through ferrocene arms 4 and 5, the inelastic excitations should occur via the LUMO+6 component of the low-lying excited states, but these excitations occur via the LUMO+5 component for ferrocene arms 1 and 2 (Fig. 1e; see Supplementary Information). These rotations are therefore triggered by electron energy transfer through the first excited states of the molecular rotor, which are essentially built up from the molecular orbitals depending on how the tip apex is electronically coupled to the rotor (Supplementary Information).

Because the rotation is based on a ratchet mechanism, one of the two rotational directions (clockwise or anticlockwise) should have a higher probability of occurrence if an overall directional rotation is to take place. This can be determined directly from the IET quantum yield[27–29], which is related to the energy transfer rate R, the electron charge e and the tunnelling current I as $Y = Re/I$. Y reflects the fraction of a tunnelling electron used to induce rotation. For a 360° rotation of the rotor, it is necessary to check the IET yields for the 15 potential wells. Because the height profiles of the potential wells are repeated every fifth well (Fig. 4a), determination of the IET yields for five consecutive wells is sufficient to cover the whole 360° rotation (see Supplementary Information). For excitation of the truncated arm, the clockwise and anticlockwise rotation yields for the first well are almost the same (within error), whereas the remaining four wells have higher yields for clockwise rotation (Fig. 4d). For excitations of the ferrocene arms, the reverse direction (anticlockwise) has consistently higher yields for all five wells when compared with clockwise rotation (Fig. 4e). The average quantum yield for excitations at truncated arm position are $Y_{cw} = 4.14 \times 10^{-9}$ and $Y_{acw} = 1.16 \times 10^{-9}$, and that for the ferrocene excitations are $Y_{cw} = 7.78 \times 10^{-10}$ and $Y_{acw} = 1.91 \times 10^{-9}$, respectively. The low yields for the ferrocene excitations are probably due to higher energy requirements. As the rotational potentials are dissymmetric, the quantum yields for sites 1 to 5 are also different. In the case of anticlockwise rotations, the excitation may involve more than one electronic state, thereby adding further differences in quantum yields for these sites.

A unidirectional rotation demands not only a sawtooth asymmetric potential, but also the rectification of a coloured noise to provide rotational energy relative to the ambient (surface) temperature[14,32]. In the case of biological molecular motors, this process transforms chemical energy into a mechanical motion[32]. In our experiment, the IET can be considered as a shot noise source[33], which provides electronic energy to the molecule. The transferred electron energy is then transformed to a mechanical motion—that is, rotation—by vibrational relaxations. Population of the excited states occurs upon tunnelling electron energy transfers, followed by energy relaxation towards the ground state. Rectification of the corresponding shot noise requires that the relaxation time towards the ground state is longer than the electron energy transfer time[33]. In molecular excitation processes, the typical relaxation time is much slower (>1 ns) than the electron transfer time through a molecule (<1 ps). The relaxation process here can therefore be considered as filtering of the tunnelling shot noise excitation into a coloured noise excitation for the rovibronic ground states, thereby delivering the average energy required for a stepped rotation. In the case of single-molecule rotations on a Au(111) surface, the surface reconstruction can significantly complicate the rotation of the molecule[15]. In our work, however, the rotor part is lifted above the surface by the tripodal stator, so the Au(111) surface

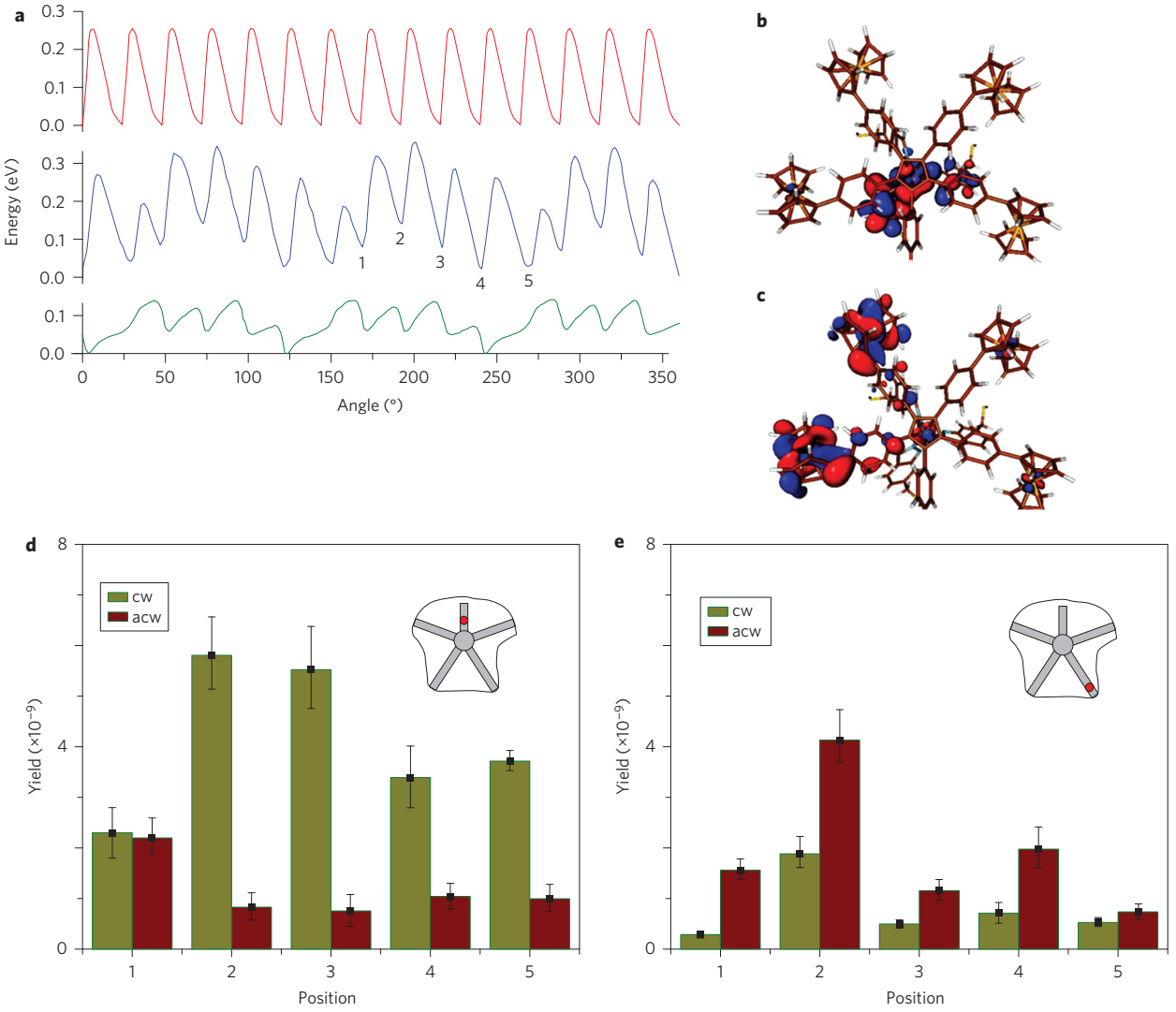

Figure 4 | Rotation mechanism. a, Fifteen uniform potential wells of the ground-state potential energy for a 360° rotation of five ferrocene arms (red). When one ferrocene is replaced by a truncated arm, it induces dissymmetry in the ground-state potentials (blue) and five potential wells (labelled 1 to 5) are repeated. An asymmetric potential simulating an excited state made of an equivalent weight contribution from LUMO+3 to LUMO+6 is shown in green. **b**, The LUMO+1 orbital located on the stator. **c**, The LUMO+6 orbital located on the rotor. **d**,**e**, IET quantum yields for excitations at the truncated arm (**d**) and for excitations at the ferrocene arms (**e**), corresponding to five potential wells marked 1 to 5 in **a**. Error bars in **d** and **e** are standard deviations from the switching rates.

does not influence the rotation. Indeed, a motor located at the corner, side or between the herringbone reconstructions produces similar results.

In summary, we report the operation of a stand-alone multicomponent molecular motor on a Au(111) surface as well as its detailed rotation mechanisms. Asymmetries in the rotation energy potential and inelastic tunnelling effects lead to unidirectional motion in both clockwise and anticlockwise directions by selectively exciting different subunits of the motor. This finding will further accelerate the development of complex and automated nanomachinery that can be operated on a material surface.

Methods

Both ASED+ and DFT methods were used to calculate the barrier to rotation for a full rotation of a single molecular rotor held away from the surface and by chemically saturating the end of the tripod with hydrogen. The two methods provided essentially similar results. Because of computational space limits, calculations for a two-layer Au(111) slab were performed using only semi-empirical ASED+ calculations[30] .

Received 27 June 2012; accepted 12 November 2012; published online 23 December 2012

References

1. Bath, J. & Turberfield, A. J. DNA nanomachines. *Nature Nanotech.* **2,** 275–284 (2007).
2. Goel, A. & Vogel, V. Harnessing biological motors to engineer systems for nanoscale transport and assembly. *Nature Nanotech.* **8,** 465–475 (2008).
3. Kottas, G. S., Clarke, L. I., Horinek, D. & Michl, J. Artificial molecular rotors. *Chem. Rev.* **105,** 1281–1376 (2005).
4. Van Delden, R. A. *et al.* Unidirectional molecular motor on a gold surface. *Nature* **437,** 1337–1340 (2005).
5. Liu, M., Zentgraf, T., Liu, Y. M., Bartel, G. & Zhang, X. Light-driven nanoscale plasmonic motors. *Nature Nanotech.* **8,** 570–573 (2010).
6. Ruangsupapichat, N., Pollard, M. M., Harutyunyan, S. R. & Feringa, B. L. Reversing the direction in a light-driven rotary molecular motor. *Nature Chem.* **3,** 53–60 (2011).
7. Hernandez, J. V., Kay, E. R. & Leigh, D. A. A reversible synthetic rotary molecular motor. *Science* **306,** 1532–1537 (2004).
8. Kelly, T. R., Silva, R. A., De Silva, H., Jasmin, S. & Zhao, Y. J. A rotationally designed prototype of a molecular motor. *J. Am. Chem. Soc.* **122,** 6935–6949 (2000).

9. Chen, L., Nakamura, M., Schindler, T. D., Parker, D. & Bryant, Z. Engineering controllable bidirectional molecular motors based on myosin. *Nature Nanotech.* **7,** 252–256 (2012).
10. Lee, L. K., Ginsburg, M. A., Crovace, C., Donohoe, M. & Stock, D. Structure of the torque ring of the flagellar motor and the molecular basis for the rotational switching. *Nature* **466,** 996–1000 (2010).
11. Uchihashi, T., Iino, R., Ando, T. & Noji, H. High-speed atomic force microscopy reveals rotary catalysis of rotorless F_1-ATPase. *Science* **333,** 755–758 (2011).
12. Tierney, H. L. *et al.* Experimental demonstration of a single-molecule electric motor *Nature Nanotech.* **6,** 625–629 (2011).
13. Kudernac, T. *et al.* Electrically driven directional motion of a four-wheeled molecule on a metal surface. *Nature* **479,** 208–211 (2011).
14. Astumian, R. D. Thermodynamics and kinetics of a Brownian motor. *Science* **276,** 917–922 (1997).
15. Manzano, C. *et al.* Step-by-step rotation of a molecule-gear mounted on an atomic-scale axis. *Nature Mater.* **8,** 576–579 (2009).
16. Wickham, S. F. J. *et al.* Direct observation of stepwise movement of a synthetic molecular transporter. *Nature Nanotech.* **6,** 166–169 (2011).
17. Shirai, Y., Osgood, A. J., Zhao, Y. M., Kelly, K. F. & Tour, J. M. Directional control in thermally driven single-molecule nanocars. *Nano Lett.* **5,** 2330–2334 (2005).
18. Vives, G. & Rapenne, G. Directed synthesis of symmetric and dissymmetric molecular motors built around a ruthenium cyclopentadienyl tris(indazolyl)borate complex. *Tetrahedron* **64,** 11462–11468 (2008).
19. Vives, G., de Rouville, H. P. J., Carella, A., Launay, J. P. & Rapenne, G. Prototypes of molecular motors based on star-shaped organometallic ruthenium complexes. *Chem. Soc. Rev.* **38,** 1551–1561 (2009).
20. Joachim, C. *et al.* Multiple atomic scale solid surface interconnects for atom circuits and molecule logic gates. *J. Phys. Condens. Matter* **22,** 084025 (2010).
21. Stipe, B. C., Razaei, M. A. & Ho, W. Coupling of vibrational excitation to the rotational motion of a single adsorbed molecule. *Phys. Rev. Lett.* **81,** 1263–1266 (1988).
22. Sainoo, Y., Kim, Y., Komeda, T., Kawai, M. & Shigekawa, H. Observation of cis-2-butene molecule on Pd(110) by cryogenic STM: site determination using tunneling-current-induced rotation. *Surf. Sci.* **536,** L403–L407 (2003).
23. Henningsen, N. *et al.* Inducing the rotation of a single phenyl ring with tunneling electrons. *J. Phys. Chem. C* **111,** 14843–14848 (2007).
24. Wahl, M., Stohr, M., Spillmann, H., Jung, T. A. & Gade, L. H. Rotation–libration in a hierarchic supramolecualr rotor–stator system. *Chem. Commun.* **13,** 1349–1351 (2007).
25. Tanaka, H. *et al.* Molecular rotation in self-assembled multidecker porphyrin complexes. *ACS Nano* **5,** 9575–9582 (2011).
26. Hla, S. W. STM single atom/molecule manipulation and its application to nanoscience and technology. *J. Vac. Sci. Technol. B* **23,** 1351–1360 (2005).
27. Parschau, M., Passerone, D., Rieder, K.-H., Hug, H. J. & Ernst, K.-H. Switching the chirality of single adsorbate complexes. *Angew. Chem. Int. Ed.* **48,** 4065–4068 (2009).
28. Iancu, V. & Hla, S. W. Realizing of a four-step molecular switch in scanning tunneling microscope manipulation of single chlorophyll-a molecules. *Proc. Natl Acad. Sci. USA* **103,** 13718–13721 (2006).
29. Pascual, J. I., Lorente, N., Song, Z., Conrad, H. & Rust, H. P. Selectivity in vibrationally mediated single-molecule chemistry. *Nature* **423,** 525–528 (2003).
30. Ample, F. & Joachim, C. A semi-empirical study of polyacene molecules adsorbed on a Cu(110) surface. *Surf. Sci.* **600,** 3243–3251 (2006).
31. Astumian, R. D. & Bier, M. Mechanochemical coupling of the motion of molecular motors to ATP hydrolysis. *Bio. Phys.* **70,** 637–653 (1996).
32. Ait-Haddou, R. & Herzog, W. Brownian ratchet model of molecular motors. *Cell Biochem. Biophys.* **38,** 191–213 (2003).
33. Lee, H. & Levitov, L. S. Current fluctuations in a single tunnel junction. *Phys. Rev. B* **53,** 7383–7391 (1996).

Acknowledgements

The authors acknowledge financial support from the AUTOMOL project (ANR 09-NANO-040) for molecular motor synthesis and calculations, the US Department of Energy (BES grant DE-FG-02-02ER46012) for the work of the Ohio University team (U.G.E.P., H.K., Y.Z. and S.-W. H), the A*STAR Atom Tech VIP programme phase III (2011–2014), CNRS and the University Paul Sabatier of Toulouse. G.V. acknowledges the French Ministry of National Education and the Ecole Normale Supérieure of Lyon for a PhD fellowship. The authors also thank I.M. Dixon for comments on the manuscript. This paper is dedicated to the 70th birthday of Karl-Heinz Rieder and to the 60th birthday of François Diederich.

Author contributions

S.W.H., C.J. and G.R. conceived and designed the research project. U.G.E.P., H.K. and Y.Z performed the STM experiments. F.A., M.G. and C.J. performed calculations. J.E. and C.J. developed the theory. G.V. and G.R. synthesized the molecules. All authors discussed the results and commented on the manuscript.

Additional information

Supplementary information is available in the online version of the paper. Reprints and permission information is available online at http://www.nature.com/reprints. Correspondence and requests for materials should be addressed to S.W.H. (for STM studies), C.J. (for theory) and G.R. (for synthesis).

Competing financial interests

The authors declare no competing financial interests.